
**Figure 2.2.8**
Curved mirror set to collimate the beam.

curvature of the mirror caused by its own weight. Even then, very careful mounting and precise mechanics are required to achieve this level of accuracy. If placed in the polychromatic beam directly from the source, cooling of the mirror will be necessary.

Other mirror arrangements can be employed, such as a horizontal and vertical pair of focusing mirrors in a Kirkpatrick–Baez (Kirkpatrick & Baez, 1948) arrangement. Such a device might be used to produce a small focal spot for powder-diffraction measurements from a sample in a diamond anvil cell. Multilayer mirrors can also be found in service on certain beamlines.

#### 2.2.3.3. *Compound refractive lens*

The refractive index $n$ of a material for X-rays is given (Gullikson, 2001; Spiller, 2000) by

$$n = 1 - \delta - i\beta = 1 - \frac{r_e}{2\pi}\lambda^2 \sum_n N_n f_n,$$

where $f_n = f_1 + if_2$ is the complex scattering factor for forward scattering for atom $n$ and $N_n$ is the number of atoms of type $n$ per unit volume. $\delta$ and $\beta$ are known as the refractive index decrement and the absorption index, respectively, and vary with photon energy depending on the proximity of an absorption edge. The real part of the refractive index is therefore slightly less than 1, with $\delta$ typically of the order $10^{-6}$–$10^{-9}$ depending on the energy. Thus a hole drilled in a piece of metal can act like a conventional convex lens, as the hole has a higher refractive index than the surrounding metal. With such a small difference in $n$ between hole and metal, the focusing power is very slight; however, a series of holes (Fig. 2.2.9) can be used to focus the X-ray beam over a reasonable distance (Snigirev *et al.*, 1997, 1998). For a series of cylindrical lenses, the focal length, $f$, is given by $f = r/2N\delta$, where $r$ is the radius of the hole and $N$ is the number of holes.

Note that further away from the axis of the device the X-ray beam must pass through increasing amounts of material which absorb the radiation. Hence, only relatively small holes and apertures are possible (a maximum of a few mm in diameter) and weakly absorbing metals such as Be and Al are preferred. With hard-energy photons, Ni lenses are possible, and indeed the construction of such a device is a compromise between refractive power, absorption, aperture and the desired focal length. Such devices can be placed in the monochromatic beam or in a polychromatic beam with cooling.

Many variants of the basic scheme exist, with lenses pressed from foil with a parabolic form to eliminate spherical aberrations, with axial symmetry to focus in both the horizontal and vertical simultaneously (Lengeler *et al.*, 1999), etched *via* lithography from plastic or other material, or with a more complex profile to minimize the amount of redundant material attenuating the transmitted beam by absorption and so allowing a larger aperture. A 'transfocator' can be constructed whereby series of lenses can be accurately inserted or removed from the beam path, thus allowing the focusing power to be adjusted depending on the desired focal distance and the wavelength of the experiment (Vaughan *et al.*, 2011).

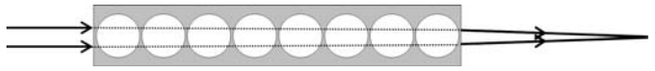

**Figure 2.2.9**
Schematic diagram of a set of refractive lenses.

### 2.2.4. Diffractometers

Most powder-diffraction beamlines are angle dispersive, operating with monochromatic radiation. When scanning a detector arm or employing a curved position-sensitive detector (PSD), detection is normally in the vertical plane because the polarization of the radiation in the plane of the synchrotron orbit means there is very little effect on the intensities due to polarization. By contrast, if diffracting in the horizontal plane, the projection of the electric vector onto the direction of the diffracted beam means that the intensity is reduced by a factor of $\cos^2 2\theta$, going to zero at $2\theta = 90°$, and so horizontal detection is less useful unless working at hard energies when $2\theta$ angles are correspondingly small. In addition, for the highest angular resolution, the natural beam divergence in the vertical plane is usually lower than in the horizontal plane, particularly if the instrument has a bending magnet or wiggler as its source.

In general, diffractometers are heavy-duty pieces of equipment and are designed to have excellent angular accuracy while working with substantial loads. A high degree of mechanical accuracy is required to match the high optical accuracy inherent in the techniques employed. The calibration of the incident wavelength and any $2\theta$ zero-point error is best done by measuring the diffraction pattern from a sample such as NIST standard Si (640 series), each of which has a certified lattice parameter (see Chapter 3.1). It is also good practice to measure the diffraction pattern of a standard sample regularly and whenever the instrument is realigned or the wavelength changed, to be sure that everything is working as expected.

Monochromatic instruments can have an analyser crystal or long parallel-foil collimators in the diffracted beam (a so-called parallel-beam arrangement), or can scan a receiving slit, or possess a one- or two-dimensional PSD, similar to Debye–Scherrer or Laue front-reflection geometry. Instruments equipped with a PSD can collect data much faster than those with a scanning diffractometer, so are exploited especially for time-resolved measurements. They may also have advantages for rapid data collection if the sample is sensitive to radiation, or be helpful if the sample is prone to granularity or texture to assess the extent of the problem.

Instruments can also be equipped with a sample changer, allowing measurements on a series of specimens, perhaps prepared by systematically changing the conditions of synthesis or the composition in a combinatorial approach. The use of beam time can be optimized with minimal downtime due to interventions around the instrument, and with the possibility to control the data acquisition remotely if desired.

#### 2.2.4.1. *Parallel-beam instruments*

Cox *et al.* (1983, 1986), Hastings *et al.* (1984) and Thompson *et al.* (1987) described the basic ideas behind these instruments *via* their pioneering work at CHESS (Cornell, USA) and NSLS (Brookhaven, USA). The highly collimated monochromatic

incident beam is diffracted by the sample and passes *via* a perfect analyser crystal [such as Si or Ge(111)] to the detector. The analyser crystal defines a very narrow angular acceptance for the diffracted radiation, determined by its Darwin width. The combination of the collimation of the incident radiation, its highly monochromatic nature and the stringent angular acceptance defines the instrument's excellent angular resolution. The detector arm supporting the analyser is scanned through the desired range of $2\theta$ angles either in a step-scan mode or continuously, reading out at very short intervals the electronic modules that accumulate the detector counts.

To be transmitted by the analyser crystal, a photon must be incident on the crystal at the correct angle $\theta_a$ that satisfies the Bragg condition. The analyser crystal defines therefore a true direction ($2\theta$ angle) for the diffracted beam irrespective of where in the sample it originates from. This removes a number of aberrations that affect diffractometers with a scanning slit or PSD where the $2\theta$ angle is inferred from the position of the slit or detecting pixel. Thus, with a capillary specimen, peak widths are independent of the capillary diameter, so a fat capillary of non-absorbing sample can be used to optimize diffracted intensity, and any modest misalignment of the sample from the diffractometer axis, or specimen transparency or surface roughness for flat-plate samples, does not lead to shifts in the peak positions. Modest movement of the sample with temperature changes in a furnace *etc*. does not cause shifts in peak positions. These instruments are therefore highly accurate, and are ideal for obtaining peak positions for indexing a diffraction pattern of a material of unknown unit cell (the first step in the solution of a structure from powder data), or following the evolution of lattice parameter with temperature *etc*. For flat samples, the $\theta/2\theta$ parafocusing condition does not need to be satisfied to have high resolution. The peak width does not therefore depend on sample orientation, which is useful for measurements of residual strain by the $\sin^2\psi$ technique or for studying surfaces and surface layers by grazing-incidence diffraction. Interchange between capillary and flat-plate samples can easily be done as required without major realignment of the instrument. The stringent acceptance conditions also help to suppress parasitic scattering originating from sample-environment windows *etc*. and inelastic scattering such as fluorescence and Compton scattering.

On the other hand, at any $2\theta$ angle only a tiny fraction of the diffracted photons can be transmitted by an analyser crystal, so this is a technique that consumes a lot of photons, and the high incident flux is essential to keep scan times to reasonable values. To overcome this, at least to some extent, Hodeau *et al.* (1998) devised a system of multiple analyser crystals, with nine channels mounted in parallel, each separated from the next by 2° (Fig. 2.2.10). In effect, as the detector arm is scanned, nine high-resolution powder-diffraction patterns are measured in parallel, each offset from the next by 2°. If the data from the channels are to be combined, which is the usual procedure, the detectors must be calibrated with respect to each other, in terms of counting efficiency and exact angular offset, by comparing regions of the diffraction pattern scanned by several detectors (Wright *et al.*, 2003). A multianalyser system speeds up data collection significantly and can be found in various modified forms at a number of powder-diffraction beamlines (*e.g.* Lee, Shu *et al.*, 2008).

The multianalyser approach is best suited to capillary samples because of the axial symmetry of the arrangement. With flat plates in reflection, only one detector can be in the $\theta/2\theta$ condition where the effect of specimen absorption (for a sufficiently thick sample) is isotropic. Corrections must therefore be made to the intensities from the other channels (Lipson, 1967; Koopmans & Rieck, 1968). For a capillary, choosing the wavelength and the diameter allows absorption to be kept to an acceptable value. Maximum diffracted intensity is expected at $\mu r = 1$ (where $\mu$ is the linear absorption coefficient and $r$ the radius of the capillary), and below this value simple absorption corrections can be applied (Hewat, 1979; Sabine *et al.*, 1998). A value of $\mu r$ greater than 1.5 begins to degrade the quality of the pattern significantly. If a sample with high absorption is unavoidable, such as when working close to an absorption edge of an element, *e.g.* the *K* edge of Mn at 6.539 keV (1.896 Å), then it can be preferable to stick a thin layer of sample on the outside of a 1-mm-diameter capillary. The shell-like nature of the sample has no effect on the peak shape or resolution because of the use of analyser crystals.

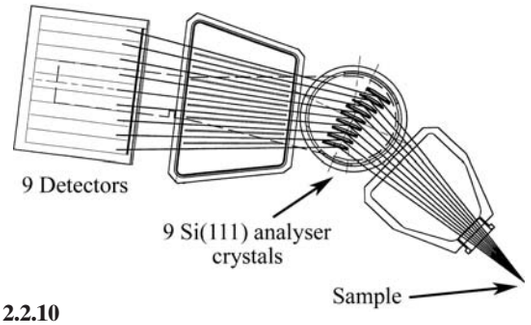


**Figure 2.2.10**
Multianalyser stage, nine channels separated by 2°, devised by Hodeau *et al.* (1998), originally installed on the BM16 bending-magnet beamline at the ESRF with Ge(111) analyser crystals. With an undulator source, the greatly increased flux allows use of Si(111), which has a narrower Darwin width (by a factor of ∼2.4) and thus improved $2\theta$ resolution, but with a lower fraction of the diffracted radiation accepted.

Capillaries also have the advantage that preferred orientation can be significantly less as compared to a flat sample, where there is a tendency for crystallites to align in the surface layers, especially if compressed to hold the powder in place. Spinning or otherwise moving the sample is necessary, whether capillary or flat plate, to increase the number of crystallites appropriately oriented to fulfil the Bragg condition and avoid a spotty diffraction pattern, the likelihood of which is exacerbated by the highly collimated nature of the incident radiation.

#### 2.2.4.1.1. *Angular resolution*

Various authors (*e.g.* Sabine, 1987*a*,*b*; Wroblewski, 1991; Masson *et al.*, 2003; Gozzo *et al.*, 2006) have discussed the resolution of a synchrotron-based diffractometer equipped with a double-crystal monochromator and an analyser crystal. The most usual setting of the diffracting crystals, ignoring any mirrors or other optical devices, is non-dispersive, alternatively described as parallel or (1, −1, 1, −1).

The approach developed by Sabine (1987*a*,*b*) involves modelling the vertical divergence of the source and the angular acceptance of the monochromator and analyser crystals as Gaussian distributions with the same full width at half-maximum (FWHM) as the real distributions, and considering a powder as a crystal with an infinite mosaic spread. The rocking curve of the analyser crystal (equivalent to rocking $2\theta$) is given by

$$I(\beta) = \int\int \mathrm{d}\alpha\,\mathrm{d}\delta \exp\left\{-\left[\left(\frac{\alpha}{\alpha'_m}\right)^2 + 2\left(\frac{\delta-\alpha}{\Delta'_m}\right)^2 + \left(\frac{b\delta+\alpha-\beta}{\Delta'_a}\right)^2\right]\right\},$$

where

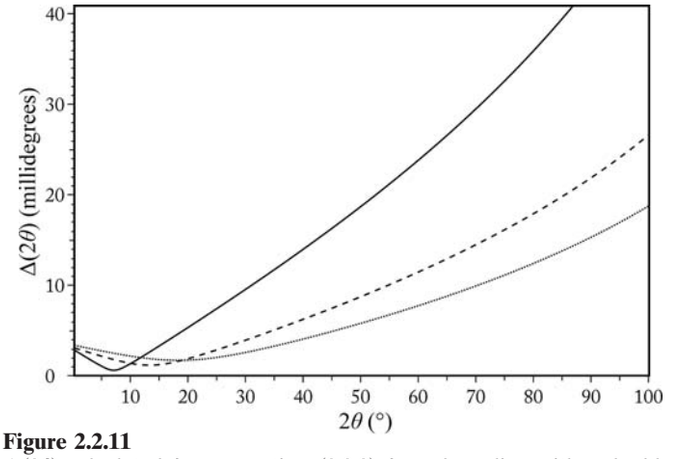


**Figure 2.2.11**
$\Delta(2\theta)$ calculated from equation (2.2.2) for a beamline with a double-crystal Si(111) monochromator, an Si(111) analyser ($\Delta_m = \Delta_a$ and $\theta_m = \theta_a$) and an FWHM vertical divergence of 25 μrad at $\lambda = 0.4$ Å (solid line: $\Delta_m \simeq 8.3$ μrad, $\theta_m = 3.6571°$), $\lambda = 0.8$ Å (dashed line: $\Delta_m \simeq 16.6$ μrad, $\theta_m = 7.3292°$) and $\lambda = 1.2$ Å (dotted line: $\Delta_m \simeq 25.2$ μrad, $\theta_m = 11.0319°$).

$$b = \tan\theta_a/\tan\theta_m - 2\tan\theta/\tan\theta_m.$$

Here $\alpha$ represents the vertical divergence from the source, $\delta$ is the difference between the Bragg angles of a central ray reflected from the monochromator at the angle $\theta_m$ and of another ray at angle $\theta'_m$ such that $\delta = \theta'_m - \theta_m$, and $\theta_a$ is the Bragg angle of the analyser crystal. The terms $\alpha'_m$, $\Delta'_m$ and $\Delta'_a$ are related to the FWHM of the Gaussians representing the vertical divergence distribution or the Darwin widths of the monochromator and analyser crystals, $\alpha_m$, $\Delta_m$ and $\Delta_a$, respectively, with

$$\alpha'_m = \alpha_m/2(\ln 2)^{1/2}, \quad \Delta'_m = \Delta_m/2(\ln 2)^{1/2}, \quad \Delta'_a = \Delta_a/2(\ln 2)^{1/2}.$$

From the above equation, the intrinsic FWHM of the Gaussian-approximated peaks of the powder-diffraction pattern can be obtained as

$$\Delta^2(2\theta) = \alpha_m^2\left(\frac{\tan\theta_a}{\tan\theta_m} - 2\frac{\tan\theta}{\tan\theta_m} + 1\right)^2 + \tfrac{1}{2}\Delta_m^2\left(\frac{\tan\theta_a}{\tan\theta_m} - 2\frac{\tan\theta}{\tan\theta_m}\right) + \Delta_a^2. \quad (2.2.2)$$

Note that the true peak shape is not Gaussian, and a pseudo-Voigt (*e.g.* as described by Thompson *et al.*, 1987), Voigt (*e.g.* Langford, 1978; David & Matthewman, 1985; Balzar & Ledbetter, 1993) or other function modelled from first principles (*e.g.* Cheary & Coelho, 1992; Ida *et al.*, 2001, 2003) is usually better. Examples of FWHM curves calculated from equation (2.2.2) are plotted in Fig. 2.2.11 at three wavelengths. Differentiating the Bragg equation gives $\Delta d/d = -\cot\theta\,\Delta(\theta)$, where $\theta$ is in radians.

Gozzo *et al.* (2006) have extended the formulation of Sabine to include the effects of collimating and focusing mirrors in the overall scheme. Axial (horizontal) divergence of the beam between the sample and the detector causes shifts and broadening of the peaks, as well as the well known low-angle peak asymmetry due to the curvature of the Debye–Scherrer cones. Sabine (1987*b*), based on the work of Hewat (1975) and Hastings *et al.* (1984), suggests the magnitude of the broadening, $B(2\theta)$, due to horizontal divergence $\Phi$ can be estimated *via*

$$B(2\theta) = (\tfrac{1}{4}\Phi)^2(\cot 2\theta + \tan\theta_a),$$

where $B$ and $\Phi$ are in radians. This value is added to $\Delta(2\theta)$.

#### 2.2.4.1.2. *Hart–Parrish design*

A variant of the parallel-beam scheme replaces the analyser crystal with a set of long, fine Soller collimators (Parrish *et al.*, 1986; Parrish & Hart, 1987; Parrish, 1988; Cernik *et al.*, 1990; Collins *et al.*, 1992) (Fig. 2.2.12). The collimators define a true angle of diffraction, but with lower $2\theta$ resolution than an analyser crystal because their acceptance angle is necessarily much larger and so the transmitted intensity is greater. They are not particularly suitable for fine capillary specimens, as the separation between foils may be similar to the capillary diameter, resulting in problems of shadowing of the diffracted beam. However, they are achromatic, and so do not need to be reoriented at each change of wavelength, which may have advantages when performing anomalous-scattering studies around an element's absorption edge. Unlike an analyser crystal, however, they do not suppress fluorescence. Peak shapes and resolution can be influenced by reflection of X-rays from the surface of the foils, or any imperfections in their manufacture, *e.g.* if the blades are not straight and flat. The theoretical resolution curve of such an instrument can be obtained from equation (2.2.2) by setting $\tan\theta_a$ to zero and replacing the angular acceptance of the analyser crystal $\Delta_a$ with the angular acceptance of the collimator $\Delta_c$.

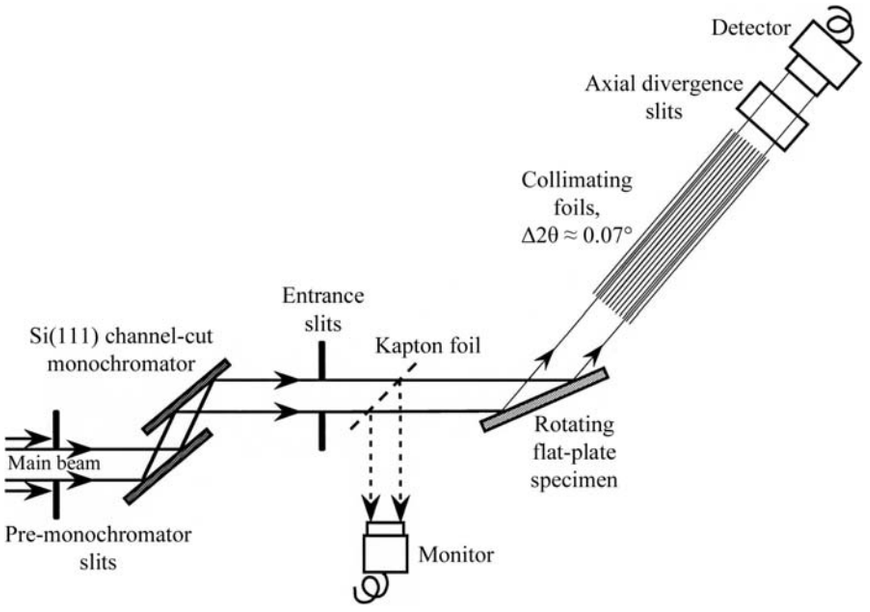


**Figure 2.2.12**
Schematic representation of a parallel-beam diffractometer of the Hart–Parrish design. The collimators installed on Stations 8.3 and 2.3 at the SRS Daresbury (Cernik *et al.*, 1990; Collins *et al.*, 1992) had steel blades 50 μm thick, 355 mm long, separated by 0.2 mm spacers, defining a theoretical opening angle (FWHM $\Delta_c$) of 0.032° and a transmission of 80%.

#### 2.2.4.2. *Debye–Scherrer instruments*

The simplest diffractometer has a receiving slit at a convenient distance from the sample in front of a point detector such as a scintillation counter. The height of the slit should match the capillary diameter, or incident beam height for flat plates. A slightly larger antiscatter slit near the sample should also be employed to reduce

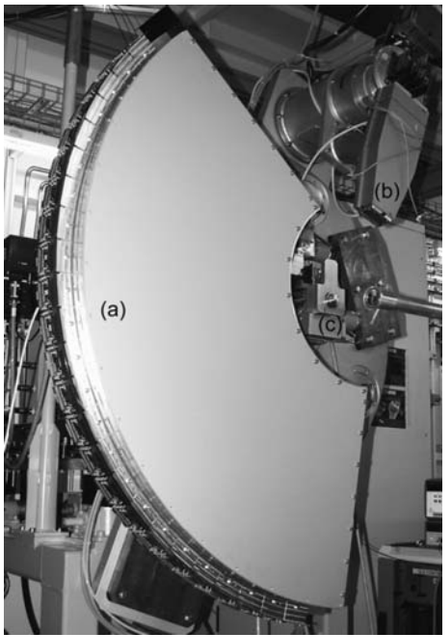


**Figure 2.2.13**
(*a*) 120° Mythen detector box, containing helium, mounted on the powder diffractometer of the materials science beamline at the Swiss Light Source. (*b*) Multianalyser detector stage. (*c*) Capillary spinner. (Bergamaschi *et al.*, 2009, 2010.)

background. The detector arm is scanned and a powder pattern recorded. This arrangement can be used for narrow capillary samples on lower-flux sources, avoiding the loss of intensity that use of an analyser crystal entails. The resolution is largely determined by the opening angle defined by the capillary and the receiving slit. Despite the simplicity of such an instrument, high-quality high-resolution data can be obtained.

For much faster data acquisition, a one-dimensional (1D) PSD or an area detector can be employed. Any sort of 1D detector with an appropriate number of channels, channel separation, efficiency, count rate (in an individual channel and overall) and speed of read out can be employed. Technology evolves and detectors make continual progress in performance. At the time of writing the most advanced 1D detector is the Mythen module developed by the Swiss Light Source (SLS). Mythen modules are based on semiconducting silicon technology and have 1280 8-mm-wide strips with a 50 μm pitch (64 × 8 $mm^2$). They can be combined to form very large curved detectors such as that on the powder diffractometer of the materials science beamline at the SLS (Fig. 2.2.13). This detector consists of 24 modules, 30 720 channels, set on a radius of 760 mm, covering 120° $2\theta$. Detector elements are therefore separated by ∼0.004°. The whole detector can be read out in 250 μs. Being Si based, its efficiency falls off above 20–25 keV, where the absorbing power of Si falls to very small values. Nevertheless, at intermediate and low energies a full powder-diffraction pattern for structural analysis can be measured in just seconds, or even faster if the intention is to follow a dynamic process.

Two-dimensional (2D) detectors are generally flat, so cannot extend to the same $2\theta$ values as a curved multistrip detector unless scanned on a detector arm. This is possible, but usually a short wavelength is used with a fixed detector. This allows an adequate data range to be recorded, particularly if the detector is positioned with the direct beam ($2\theta = 0$) near an edge. A 2D detector records complete or partial Debye–Scherrer rings, which increases the counting efficiency with respect to scanning an analyser crystal by several orders of magnitude. In addition, if the rings do not appear smooth and homogeneous, this indicates problems with the sample, such as preferred orientation or granularity, both of which can seriously affect diffraction intensities when measuring just a thin vertical strip. Detectors that have been used are diverse and include image plates, though these have slow read out, charge-coupled devices (CCDs) or Si-based photon-counting pixel detectors used for single-crystal diffraction or protein crystallography (*e.g.* Broennimann *et al.*, 2006), and medical-imaging detectors, which are designed for hard-energy operation. Examples include the CCD-based Frelon camera, developed at the ESRF (Labiche *et al.*, 2007), and commercially available large flat-panel medical-imaging detectors up to 41 × 41 $cm^2$, based on scintillator-coated amorphous silicon, which have been exploited at speeds of up to 60 Hz for selected read-out areas (Chupas, Chapman & Lee, 2007; Lee, Aydiner *et al.*, 2008; Daniels & Drakopoulos, 2009).

Note that a 2D detector can be used as a 1D detector by applying a mask and reading out only a narrow strip, which can enhance the rate of data acquisition. For CCD chips, the electronic image can be rapidly transferred to pixels behind the masked part of the detector from where it can be read out while the active area is re-exposed. Translating an image plate behind a mask is a simple way of acquiring a series of diffraction patterns for following a process with modest time resolution.

These instruments are vulnerable to aberrations that cause systematic shifts in peak positions, such as misalignment of the capillary or surface of the sample from the diffractometer axis, and specimen transparency, which also affects the peak width and shape. The peak width also depends on whether a flat sample is in the $\theta/2\theta$ condition, or on the diameter of a capillary sample, *etc*. Focusing the incident beam onto the detector decreases the peak width, as fewer pixels are illuminated compared to using a highly collimated incident beam. PSDs are much more open detectors than those behind an analyser crystal or set of slits, so are more susceptible to background and parasitic scatter from sample environments *etc*. However, the speed and efficiency of data acquisition usually outweigh such concerns.

#### 2.2.4.3. *Energy-dispersive instruments*

The broad, continuous spectrum from a wiggler or bending magnet is suitable for energy-dispersive diffraction (EDD). Here, the detector is fixed at an angle $2\theta$ and the detector determines the energy, $\varepsilon$, of each arriving photon scattered by the sample (Fig. 2.2.14). The energy [keV] can be converted to $d$-spacing [Å] *via*

$$d \simeq 12.3984/2\varepsilon \sin\theta.$$

The detector usually consists of a cryogenically cooled semiconducting Ge diode. An absorbed X-ray photon promotes electrons to the conduction band in proportion to its energy. By

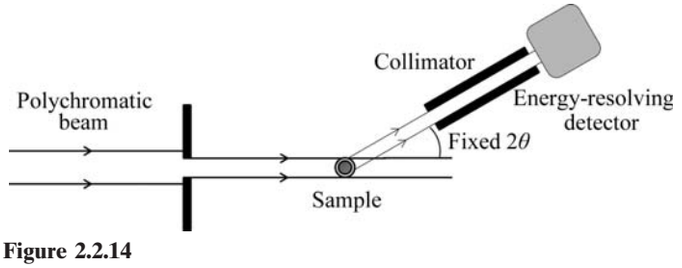


**Figure 2.2.14**
Schematic representation of an energy-dispersive diffraction arrangement.

analysing the size of the charge pulse produced, the energy of the photon is determined. The powder-diffraction pattern is recorded as a function of energy (typically somewhere within the range 10–150 keV, depending on the source) *via* a multichannel analyser (MCA). Instruments may have multiple detectors, at different $2\theta$ angles covering different ranges in $d$-spacing (Barnes *et al.*, 1998), or arranged around a Debye–Scherrer ring, as in the 23-element semi-annular detector at beamline I12 at Diamond Light Source (Korsunsky *et al.*, 2010; Rowles *et al.*, 2012).

Prior to performing the EDD experiment, the detector and MCA system must be calibrated, *e.g.* by measuring signals from sources of known energy, such as $^{241}$Am (59.5412 keV) or $^{57}$Co (122.06014 and 136.4743 keV) at hard energies, and/or from the fluorescence lines of elements such as Mo, Ag, Ba *etc*. The $2\theta$ angle also needs to be calibrated if accurate $d$-spacings are desired. This should be done by measuring the diffraction pattern of a standard sample with known $d$ values.

The detector angle is typically chosen in the range 2–6° $2\theta$ and influences the range of $d$-spacings accessible *via* the term $1/\sin\theta$, *i.e.* the lower the angle, the higher the energy needed to access any particular $d$. Normally, the range of most interest should be matched to the incident spectrum, taking account also of sample absorption and fluorescence, to produce peaks with high intensity. More than one detector at different angles can also be employed. Energy-sensitive Ge detectors do not count particularly fast, up to 50 kHz being a typical value compared to possibly 1–2 MHz with a scintillation detector. Hence they are relatively sensitive to pulse pile-up and other effects of high count rates (Cousins, 1994; Laundy & Collins, 2003; Honkimäki & Suortti, 2007), particularly if the synchrotron is operating in a mode with a few large electron bunches giving very intense pulses of X-rays on the sample.

The energy resolution of the detector is of the order of 2%, which dominates the overall resolution of the technique. Its main uses are where a fixed geometry with penetrating X-rays is required, *e.g.* in high-pressure cells, for *in situ* studies (Häusermann & Barnes, 1992), *e.g.* of chemical reactions under hydrothermal conditions (Walton & O'Hare, 2000; Evans *et al.*, 1995), electrochemistry (*e.g.* Scarlett *et al.*, 2009; Rijssenbeek *et al.*, 2011; Rowles *et al.*, 2012), or measurements of residual strain (Korsunsky *et al.*, 2010). Owing to the use of polychromatic radiation, the technique has very high flux on the sample and can be used for high-speed data collection, following rapid processes *in situ*. However, accurate modelling of the intensities of the powder-diffraction pattern for structural or phase analysis is difficult because of the need to take several energy-dependent effects into account, *e.g.* absorption and scattering factors, the incident X-ray spectrum, and the detector response. Nevertheless, examples where this has been successfully carried out have been published (*e.g.* Yamanaka & Ogata, 1991; Scarlett *et al.*, 2009).

A higher-resolution variant of the energy-dispersive technique can be performed by using a standard detector behind a collimator at fixed $2\theta$ scanning the incident energy *via* the monochromator. The Hart–Parrish design with long parallel foils is suitable. Such an approach has been demonstrated in principle (Parrish, 1988), but is rarely used in practice. The advantage is to be able to measure data of improved $d$-spacing resolution, as compared to using an energy-dispersive detector, from sample environments with highly restricted access. In principle, as a further variant, white incident radiation could be used with scanning of $\theta_a$, the angle of the analyser crystal, and associated detector at $2\theta_a$, all at fixed $2\theta$.

#### 2.2.5. Considerations for powder-diffraction experiments

Synchrotron radiation allows considerable flexibility for a powder-diffraction experiment, offering choice and optimization of a number of quantities such as the wavelength, with high energy resolution, range in $d$-spacing, angular resolution, angular accuracy, and spatial or time resolution (but not all of these can necessarily be optimized at the same time). Increasingly, powder-diffraction experiments at synchrotrons are combined with complementary measurements, simultaneously applying techniques such as Raman spectroscopy (Boccaleri *et al.*, 2007; Newton & van Beek, 2010), particularly when carrying out *in situ* studies of an evolving system. In this respect, the open nature of a synchrotron instrument, with space around the sample to position auxiliary equipment, is an advantage.

##### 2.2.5.1. *Polarization*

Assuming the beam is 100% polarized in the horizontal plane of the synchrotron orbit and with detection in the vertical plane, there is no need for any polarization correction to the diffracted intensities. However, if a small amount of vertical polarization of the beam does need to be taken into account (possibly up to a few per cent depending on the source), the polarization factor that describes its effect on the intensity of the diffracted beam can be derived, following the approach of Azároff (1955) and Yao & Jinno (1982), as

$$P = \frac{1 - dp + dp\cos^2 2\theta\cos^2 2\theta_a}{1 - dp + dp\cos^2 2\theta_a} = \frac{1 - dp + dp\cos^2 2\theta\cos^2 2\theta_a}{1 - dp\sin^2 2\theta_a}, \tag{2.2.3}$$

where $dp$ is the depolarization fraction (*i.e.* the fraction of the total intensity incident on the sample that is vertically polarized), $2\theta_a$ is the Bragg angle of the analyser crystal (if any), and the denominator scales $P$ to unity at $2\theta$ equal to zero (Dwiggins, 1983) and is a constant for any particular experimental setup. If there is no analyser crystal, or we ignore the effect it would have (*i.e.* by putting $2\theta_a = 0$), then

$$P = 1 - dp\sin^2 2\theta.$$

Beamline staff can usually advise on the appropriate values to use. These expressions reduce to the usual polarization factor for unpolarized ($dp$ = 0.5) laboratory X-rays without a monochromator or analyser crystal, $\frac{1}{2}(1 + \cos^2 2\theta)$.

An alternative formulation of equation (2.2.3) considers the ratio of the vertical to horizontal polarization,

$$rp = \frac{dp}{1 - dp} \quad \text{and} \quad dp = \frac{rp}{1 + rp},$$

so that

$$P = \frac{1 + rp\cos^2 2\theta\cos^2 2\theta_a}{1 + rp\cos^2\theta_a}. \tag{2.2.4}$$

Note that $rp$ = 1.0 for unpolarized (laboratory) X-rays. In reality, because the synchrotron beam is near 100% plane polarized, $dp$ and $rp$ have similar values. The same expressions can be used if diffracting and analysing in the horizontal plane, except that now the value of $dp$ or $rp$ is replaced with the value of $(1 - dp)$ or $1/rp$, respectively.

For Debye–Scherrer rings detected on a 2D detector, the azimuthal angle around the ring needs to be taken into account, yielding